

---

# Swing-Up and Stabilization of a Cart Pendulum System and Stabilization of a Twin Pendulum System

Using Nonlinear Control Strategies

---

Master Thesis

Aalborg University  
Control & Automation  
Fredrik Bajers Vej 7  
DK-9220 Aalborg

by  
Niels Skov Vestergaard



Master Thesis

Control and Automation

Department of Electronic Systems

Fredrik Bajers Vej 7C

9220 Aalborg

Synopsis:

**Title:**

Swing-Up and Stabilization of a Cart Pendulum System and Stabilization of a Twin Pendulum System

**Subtitle:**

Using Nonlinear Control Strategies

**Theme:**

Nonlinear Control

**Project Period:**

Autumn 2018

**Participants:**

Niels Skov Vestergaard

**Supervisor:**

John-Josef Leth

**Pages:** ?

**Appendices:** ?

**Attachments:** ?

**Concluded:** 2019-01-16

Nam dui ligula, fringilla a, euismod sodales, sollicitudin vel, wisi. Morbi auctor lorem non justo. Nam lacus libero, pretium at, lobortis vitae, ultricies et, tellus. Donec aliquet, tortor sed accumsan bibendum, erat ligula aliquet magna, vitae ornare odio metus a mi. Morbi ac orci et nisl hendrerit mollis. Suspendisse ut massa. Cras nec ante. Pellentesque a nulla. Cum sociis natoque penatibus et magnis dis parturient montes, nascetur ridiculus mus. Aliquam tincidunt urna. Nulla ullamcorper vestibulum turpis. Pellentesque cursus luctus mauris.

Nam dui ligula, fringilla a, euismod sodales, sollicitudin vel, wisi. Morbi auctor lorem non justo. Nam lacus libero, pretium at, lobortis vitae, ultricies et, tellus. Donec aliquet, tortor sed accumsan bibendum, erat ligula aliquet magna, vitae ornare odio metus a mi. Morbi ac orci et nisl hendrerit mollis. Suspendisse ut massa. Cras nec ante. Pellentesque a nulla. Cum sociis natoque penatibus et magnis dis parturient montes, nascetur ridiculus mus. Aliquam tincidunt urna. Nulla ullamcorper vestibulum turpis. Pellentesque cursus luctus mauris.

*Publication of this report's contents (including citation) without permission from the authors is prohibited*

# Contents

<b>1</b>	<b>Introduction</b>	<b>1</b>
<b>Part I Cart Pendulum</b>		<b>2</b>
<b>2</b>	<b>System and Model</b>	<b>3</b>
2.1	System . . . . .	3
2.2	Model . . . . .	5
<b>3</b>	<b>Swing-Up Design</b>	<b>8</b>
<b>Part II Twin Pendulum</b>		<b>21</b>
<b>Appendix</b>		<b>22</b>



# 1 | Introduction

This project is concerned with developing nonlinear control strategies for a cart pendulum system and to apply these to the set-up provided in the Control and Automation Lab at Aalborg University (AAU).

The project is two part. The objective of the first part is to design a swing-up controller along with a stabilizing controller to catch the pendulum at the upright position.

In the second part an additional pendulum is attached to the cart in the setup making it a twin pendulum system. The idea is to estimate the additional state and ultimately stabilize the two pendulums in upright position.

# **Part I**

## **Cart Pendulum**

# 2 | System and Model

A brief overview of the relevant system for *Part 1* is presented in this chapter along with a model of the system.

## 2.1 System

A setup is provided by the Control and Automation Department at AAU, see Figure 2.1.

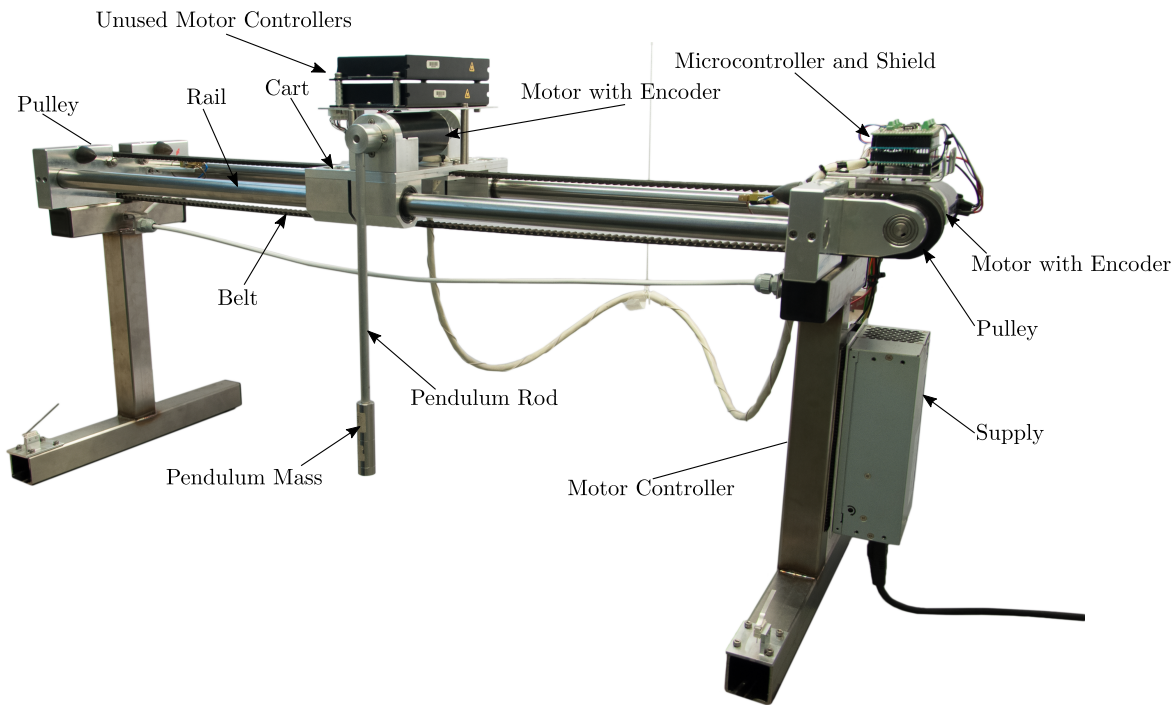


**Figure 2.1:** The setup provided by AAU. The motor controller in use is not directly visible in this picture as it is mounted behind the power supply.

As seen in Figure 2.1 the belt is attracted by pulleys one of which is driven by a brushed Maxon 370356 DC motor [1]. An other of these maxon motors is mounted on the pendulum but is disconnected and just used as a bearing in this project. Both motors are fitted with an HEDS 5540 optical quadrature encoder allowing for relative position and angle of the cart and pendulum respectively [2].

The motor driving the belt is controlled using a Maxon ADS 50/10 motor controller configured in current control mode. The motor controller takes a  $\pm 10\text{ V}$  input signal which then determines the armature current,  $i_a$ , see [3].

The primary control unit is a Teensy 3.6 microcontroller board. To program the board

through the onboard USB connection a bootloader is used along with the Teensyduino add-on for the Arduino IDE [4].

The encoders are decoded on a shield using Avago HCTL-2021-PLC decoders and read through an 8 bit parallel data bus on the microcontroller board resulting in 2000 tics pr. revolution. This ensures a resolution for the pendulum angle,  $\theta$ , of  $2\pi/2000 = \pi \times 10^{-3}$  rad/tic and  $2\pi r/2000 = 2\pi \cdot 0.028/2000 \approx 0.088 \times 10^{-3}$  m/tic for the cart position,  $x$ , see [5].

The supply circuit on the microcontroller board is powered by 5V which is regulated to 3.3 V resulting in a 0–3.3 V range for the 12 bit analog output [6]. This output is used to provide the motor controller with an armature current reference, thus, the microcontroller analog output is amplified through the shield to meet the ±10 V input requirement of the motor controller [7].

The following relation between analog 12 bit output values,  $\text{bit}_{\text{DAC}}$ , from the microcontroller and armature current in the motor was found by a previous project group [7],

$$(2.1) \quad \text{bit}_{\text{DAC}} = 105.78 \cdot i_a + 1970 ,$$

and as a result of a force test, see [8], Equation 2.1 was corrected to,

$$(2.2) \quad \text{bit}_{\text{DAC}} = 111.9 \cdot i_a + 1970 ,$$

which is the relation used in this project. All the system parameters used in the design are listed in Table 2.1. It is assumed that all frictions in the system can be modeled as a combination of Coulomb and viscous frictions. Wires hanging from the cart are unmodeled and their weight along with that of the belt are contained in the estimation of the cart mass.

Parameter	Notation	Quantity	Unit
Nominal current (max. continuous current)	$I_N$	4.58	A
Torque constant	$\tau_m$	$93.4 \times 10^{-3}$	$\text{N} \cdot \text{m} \cdot \text{A}^{-1}$
Rod Length	$l$	0.3235	m
Rail Length	$l_r$	0.89	m
Pulley Radius	$r$	0.028	m
Pendulum Mass	$m$	0.201	kg
Cart Mass	$M$	5.273	kg
Cart Coulomb Friction	$b_{c,c}$	2.884	N
Cart Viscous Friction	$b_{c,v}$	1.680	$\text{N} \cdot \text{m}^{-1} \cdot \text{s}$
Pendulum Coulomb Friction	$b_{p,c}$	0.004	N·m
Pendulum Viscous Friction	$b_{p,v}$	$0.4 \times 10^{-3}$	$\text{N} \cdot \text{m} \cdot \text{s}$

**Table 2.1:** The motor parameters,  $I_N$  and  $\tau_m$ , are given by maxon in [1]. The rod length is measured from the pendulum pivot point to the geometrical center of the pendulum. Pendulum mass, rod length, pulley radius and rail length are measured parameters, while cart mass is estimated same as all frictions. The estimations are performed by a previous project group [7].

## 2.2 Model

The model is based on the generalized coordinates presented in Figure 2.2.

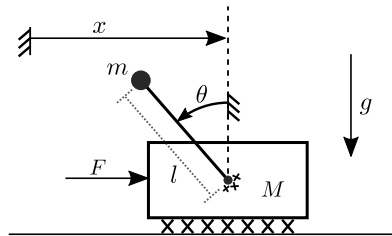


**Figure 2.2:** Mechanical drawing of the system, where  $\theta$  is the angle of the pendulum,  $x$  is the position of the center of the cart along the rail,  $F$  is the applied force and  $g$  is the gravitational acceleration. It is indicated that friction is modeled between cart and rail as well as in the pendulum joint.

The pendulum mass center is positioned at zero height at rest s.t. all energies in the system are positive. It is assumed that the pendulum rod is rigid and massless and that the pendulum weights are a point mass at the geometrical center of the weights.

The motor torque is given by direct relation to the armature current by the motor constant,  $\tau_m = k_\tau i_a$ , such that,

$$(2.3) \quad F = \frac{1}{r} k_\tau i_a \quad [\text{N}] .$$

To avoid excessive notation  $u = F$  is considered to be the control input in the remaining of this thesis, while keeping in mind the relation in Equation 2.3 along with the knowledge that  $u$  must be converted to armature current in implementation.

It is well known that the potential energy,  $U$ , and the kinetic energy,  $T$ , are given by, [9]

$$(2.4) \quad U = mgl(1 + \cos \theta) \quad [\text{J}]$$

$$(2.5) \quad T = \frac{1}{2}(M + m)\dot{x}^2 - m\dot{x}l \cos \theta \dot{\theta} + \frac{1}{2}ml^2\dot{\theta}^2 \quad [\text{J}]$$

The frictions, indicated in Figure 2.2, are, as mentioned, comprised of Coulomb and viscous frictions with values stated in Table 2.1. The viscous frictions are modeled as linear functions of velocities, [10, 11]

$$(2.6) \quad b_{p,v}\dot{\theta} \quad , \quad b_{c,v}\dot{x} \quad ,$$

for the rotational and linear case respectively. The coulomb frictions are modeled as a constant with its sign depending on the signs of the velocities, such that, [10, 11]

$$(2.7) \quad \operatorname{sgn}(\dot{\theta})b_{p,c} \quad , \quad \operatorname{sgn}(\dot{x})b_{c,c} \quad .$$

This, however, introduces discontinuities at zero velocities. Thus, tanh-functions are used to obtain a continues approximation of the sign-functions,

$$(2.8) \quad \tanh(k_{\tanh}\dot{\theta})b_{p,c} \quad , \quad b_{c,v}\dot{x} - \tanh(k_{\tanh}\dot{x})b_{c,c} \quad ,$$

where  $k_{\tanh} = 250$  to increase the steepness of the tanh-functions thereby obtaining a closer approximation of the sign-functions. Finally, by use of the Lagrange-d'Alembert Principle, [9]

$$(2.9) \quad \frac{d}{dt} \frac{\partial \mathcal{L}}{\partial \dot{\mathbf{q}}} - \frac{\partial \mathcal{L}}{\partial \mathbf{q}} = \mathbf{Q} \quad ,$$

where,

$$(2.10) \quad \mathbf{q} = \begin{bmatrix} \theta \\ x \end{bmatrix} \quad , \quad \mathbf{Q} = \begin{bmatrix} -b_{p,v}\dot{\theta} - \tanh(k_{\tanh}\dot{\theta})b_{p,c} \\ \frac{1}{r}k_{\tau}i_a - b_{c,v}\dot{x} - \tanh(k_{\tanh}\dot{x})b_{c,c} \end{bmatrix} \quad ,$$

and  $\mathcal{L} = T - U$ , the dynamics of the system are found,

$$(2.11) \quad ml^2\ddot{\theta} - ml \cos \theta \ddot{x} - mgl \sin \theta = -b_{p,v}\dot{\theta} - \tanh(k_{\tanh}\dot{\theta})b_{p,c} \quad [\text{N} \cdot \text{m}]$$

$$(2.12) \quad (M + m)\ddot{x} + ml \sin \theta \dot{\theta}^2 - ml \cos \theta \ddot{\theta} = u - b_{c,v}\dot{x} - \tanh(k_{\tanh}\dot{x})b_{c,c} \quad . \quad [\text{N}]$$

By setting up the dynamic equations, Equation 2.12 and 2.11, in the following manner,

$$(2.13) \quad \begin{aligned} & \begin{bmatrix} ml^2 & -ml \cos \theta \\ -ml \cos \theta & M + m \end{bmatrix} \begin{bmatrix} \ddot{\theta} \\ \ddot{x} \end{bmatrix} + \begin{bmatrix} 0 \\ ml \sin \theta \dot{\theta}^2 \end{bmatrix} + \\ & + \begin{bmatrix} b_{p,v}\dot{\theta} + \tanh(k_{\tanh}\dot{\theta})b_{p,c} \\ b_{c,v}\dot{x} + \tanh(k_{\tanh}\dot{x})b_{c,c} \end{bmatrix} + \begin{bmatrix} -mgl \sin \theta \\ 0 \end{bmatrix} = \begin{bmatrix} 0 \\ u \end{bmatrix} \quad , \end{aligned}$$

## Chapter 2. System and Model

the general form of an m-link robot is obtained, [12, 13]

$$(2.14) \quad \mathbf{M}(\mathbf{q})\ddot{\mathbf{q}} + \mathbf{C}(\mathbf{q}, \dot{\mathbf{q}}) + \mathbf{B}(\dot{\mathbf{q}}) + \mathbf{G}(\mathbf{q}) = \mathbf{F} \quad ,$$

where,

$\mathbf{M}(\mathbf{q})$  is the inertia matrix

$\mathbf{C}(\mathbf{q}, \dot{\mathbf{q}})$  is the Coriolis and centrifugal effects

$\mathbf{B}(\dot{\mathbf{q}})$  is the friction

$\mathbf{G}(\mathbf{q})$  is the force due to gravity

$\mathbf{F}$  is the input force vector .

Choosing  $[x_1 \ x_2 \ x_3 \ x_4]^T = [\theta \ x \ \dot{\theta} \ \dot{x}]^T$  as states results in the following nonlinear state space representation,

$$(2.15) \quad \begin{bmatrix} \dot{x}_1 \\ \dot{x}_2 \\ \dot{x}_3 \\ \dot{x}_4 \end{bmatrix} = \begin{bmatrix} & & x_3 \\ & & x_4 \\ & & \mathbf{M}^{-1}(x_1)(\mathbf{F} - \mathbf{C}(x_1, x_3) - \mathbf{B}(x_3, x_4) - \mathbf{G}(x_1)) \end{bmatrix} ,$$

which is convenient when simulation the system. This representation is also used in the controller designs.

# 3 | Swing-Up Design

In this chapter four swing-up controllers are designed, all based on [14]. The pendulum is started at rest,  $\theta = \pi$ , angle convention is specified in Figure 2.2. The idea of the swing-up controller is to increase the mechanical energy in the system until it matches that of the desired end state, which is the upright position at rest, that is,  $\theta = 0$  and  $\dot{\theta} = 0$ . The minimum energy in the system is the starting position at rest, which is considered to be zero as mentioned in the *Model* section 2.2. So the target energy is  $E_{\text{eq}} = 2mgl$ , that is, the potential energy of the pendulum in the unstable equilibrium.

Consider the pendulum dynamics from Equation 2.12,

$$(3.1) \quad J\ddot{\theta} - ml \cos \theta \ddot{x}_c - mgl \sin \theta = 0 \quad , \quad [\text{N} \cdot \text{m}]$$

where  $J = ml^2$  is the inertia and the pendulum friction is assumed to be zero. This equation captures the behavior of the pendulum corresponding to some acceleration  $\ddot{x}_c$  at the pivot point. This acceleration is viewed as the control input for now. The force needed to achieve this acceleration is considered in the end of the design. It is further convenient to describe the energy of the pendulum with the coordinate frame fixed at its pivot point, see Figure 3.1.

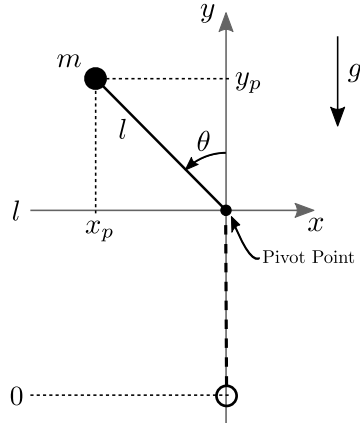


**Figure 3.1:** The energy used in the swing-up controller is described using this convention, where the coordinate frame is fixed at the pivot point of the pendulum. The zero reference is placed as before s.t. all energies are positive.

From Figure 3.1, the conversion from excessive to generalized coordinates is given by,

$$(3.2) \quad x_p = -l \sin \theta \quad , \quad y_p = l(\cos \theta + 1) \quad , \quad \dot{x}_p = -l \cos \theta \dot{\theta} \quad , \quad \dot{y}_p = -l \sin \theta \dot{\theta} \quad .$$

### Chapter 3. Swing-Up Design

The mechanical energy in this coordinate frame is then,

$$(3.3) \quad E_p = mgy_p + \frac{1}{2}m\dot{x}_p^2 + \frac{1}{2}m\dot{y}_p^2 \quad [\text{J}]$$

$$(3.4) \quad E_p = mgl(\cos \theta + 1) + \frac{1}{2}m(-l \cos \theta \dot{\theta})^2 + \frac{1}{2}m(-l \sin \theta \dot{\theta})^2 \quad [\text{J}]$$

$$(3.5) \quad E_p = mgl(\cos \theta + 1) + \frac{1}{2}J(\cos^2 \theta + \sin^2 \theta)\dot{\theta}^2 \quad [\text{J}]$$

$$(3.6) \quad E_p = \frac{1}{2}J\dot{\theta}^2 + mgl(\cos \theta + 1) \quad . \quad [\text{J}]$$

## Energy Control

A Lyapunov function candidate is proposed,

$$(3.7) \quad V = \frac{1}{2}E_\Delta^2 \quad ,$$

where  $E_\Delta$  is the difference in energy in relation to the unstable equilibrium,

$$(3.8) \quad E_\Delta = E_p - E_{\text{eq}} \quad [\text{J}]$$

$$(3.9) \quad E_\Delta = \frac{1}{2}J\dot{\theta}^2 + mgl(\cos \theta + 1) - 2mgl \quad [\text{J}]$$

$$(3.10) \quad E_\Delta = \frac{1}{2}J\dot{\theta}^2 + mgl(\cos \theta - 1) \quad . \quad [\text{J}]$$

The derivative of  $E_\Delta$  from Equation 3.10 along the system Equation 3.1 is found to,

$$(3.11) \quad \dot{E}_\Delta = J\dot{\theta}\ddot{\theta} - mgl \sin \theta \dot{\theta}$$

$$(3.12) \quad \dot{E}_\Delta = \dot{\theta}(ml \cos \theta \ddot{x}_c + mgl \sin \theta) - mgl \sin \theta \dot{\theta}$$

$$(3.13) \quad \dot{E}_\Delta = ml \cos \theta \dot{\theta} \ddot{x}_c \quad .$$

The Lyapunov function candidate, Equation 3.7, is continuously differentiable in the entire  $\mathbb{R}^{2 \times 1}$ . Its derivative is evaluated to find a stabilizing controller,

$$(3.14) \quad \dot{V} = E_\Delta \dot{E}_\Delta$$

$$(3.15) \quad \dot{V} = E_\Delta ml \cos \theta \dot{\theta} \ddot{x}_c \leq 0 \quad .$$

The acceleration,  $\ddot{x}_c$ , is then designed to satisfy the stability criterion in Equation 3.15,

$$(3.16) \quad \dot{V} = mlE_\Delta \cos \theta \dot{\theta}(-E_\Delta \cos \theta \dot{\theta})$$

$$(3.17) \quad \dot{V} = -ml(E_\Delta \cos \theta \dot{\theta})^2 \leq 0 \quad ,$$

further a tuning parameter,  $k > 0$ , is introduced such that the control law for acceleration of the pivot point is,

$$(3.18) \quad \ddot{x}_c = -kE_\Delta \cos \theta \dot{\theta} \quad .$$

If this control law is started at zero angular velocity,  $\dot{\theta} = 0$ , in a stable equilibrium, the computed control is maintained at zero and the pendulum never swings up. So for this

---

<sup>1</sup>Fixme Note: brush up on stability criteries

control law to work, the pendulum must be started slightly away from a stable equilibrium. The control is also zero when  $\cos \theta = 0$ , however, when this occurs the system is not in a stable equilibrium and the zero value of  $\ddot{x}_c$  is therefore not maintained in these cases.

An extra step is needed to apply this control strategy. So far the control output is an acceleration,  $\ddot{x}_c$ , at the pivot point. It is possible to input the desired acceleration,  $\ddot{x}_c$ , into the second dynamic equation, Equation 2.12, and solve for the force needed to achieve this acceleration,

$$(3.19) \quad u = (M + m)\ddot{x}_c + ml \sin x_1 x_3^2 - ml \cos x_1 \dot{x}_3 \quad , \quad [N]$$

where the cart friction coefficients are set to zero again.

To calculate the force from this expression, Equation 3.19, it is also necessary to know the angular acceleration of the pendulum,  $\dot{x}_3$ , which can be solved for in the system dynamics, Equation 2.15, inserting known states and control input applied in the previous step,

$$(3.20) \quad \begin{bmatrix} \dot{x}_3 \\ \dot{x}_4 \end{bmatrix} = \begin{bmatrix} ml^2 & -ml \cos x_1 \\ -ml \cos x_1 & M + m \end{bmatrix}^{-1} \begin{bmatrix} -b_{p,v}x_3 - \tanh(k_{\tanh}x_3)b_{p,c} + mgl \sin x_1 \\ u_{last} - ml \sin x_1 x_3^2 \end{bmatrix} \quad ,$$

where  $u_{last}$  is the force applied in the previous step.

From Equation 3.20 the approximated angular acceleration is then,

$$(3.21) \quad \dot{x}_3 = \frac{(M + m)(-b_{p,v}x_3 - \tanh(k_{\tanh}x_3)b_{p,c} + mgl \sin x_1)}{l^2 m(M + m - m \cos^2 x_1)} + \frac{\cos x_1(u_{last} - ml \sin x_1 x_3^2)}{l(M + m - m \cos x_1^2)} \quad .$$

Inserting Equation 3.21 into Equation 3.19 results in the control input,  $u$ , necessary to achieve the desired acceleration,  $\ddot{x}_c$ , at the pivot point. This method is used for all swing-up controllers, so to avoid excessive notation the proceeding energy control laws are derived with  $\ddot{x}_c$  as the control parameter.

All simulations are performed using the nonlinear state space representation in Equation 2.15 and the matlab ODE45 solver with relative tolerance of  $1 \times 10^{-7}$ . Initializing the angle,  $\theta$ , at  $\pi - 0.1$  to avoid zero control output as discussed, the energy difference struggles to reach its reference at zero, see Figure 3.2.

### Chapter 3. Swing-Up Design

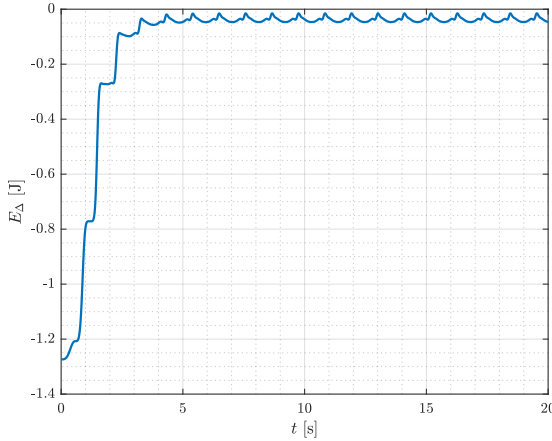


**Figure 3.2:** Edelta1noConX

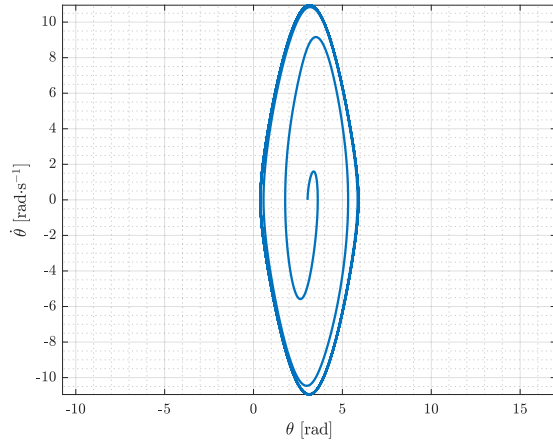


**Figure 3.3:** phase1noConX

The pendulum also falls short of reaching the heteroclinic orbit, see Figure 3.3.<sup>2</sup> Some energy is lost to friction in the pendulum. The cart however is considered to be frictionless in both design and simulation for now.<sup>3</sup> However, as the energy of the pendulum is not affected by the position or velocity of the cart, this control law, Equation 3.18, is not concerned with controlling these. This becomes a problem in the physical setup as it has a rail length of one meter. A traced animation is used to demonstrate this problem in Figure 3.4.

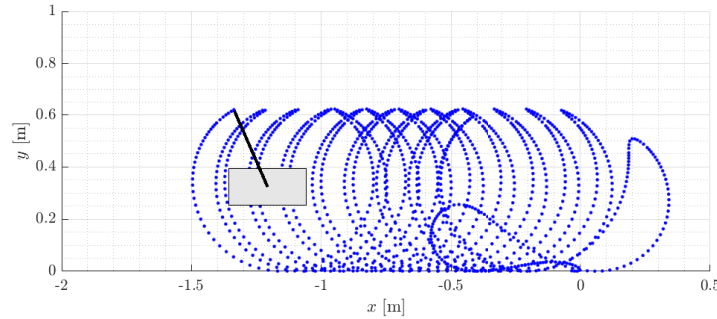


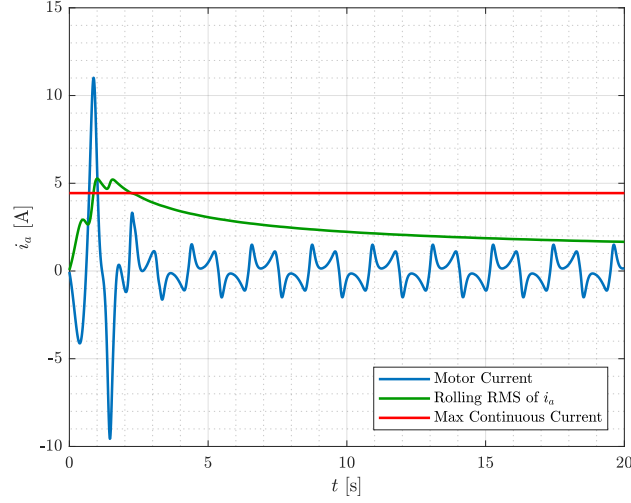
**Figure 3.4:** ani1noConX

An other issue is the actuation which is limited in the real system by the maximum allowed continuous current, see Table 2.1. By tuning the parameter  $k$  in Equation 3.18, better performance can be obtained, however at the cost of excessive actuation.

---

<sup>2</sup>FIXme Note: include small section on heteroclinic orbit

<sup>3</sup>FIXme Note: remember a section on friction compensation

**Figure 3.5:** ialnoConX

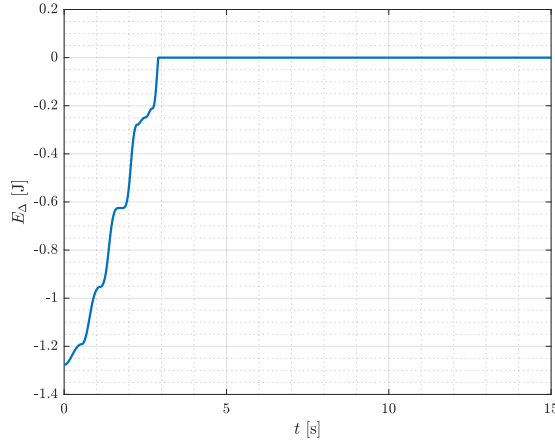
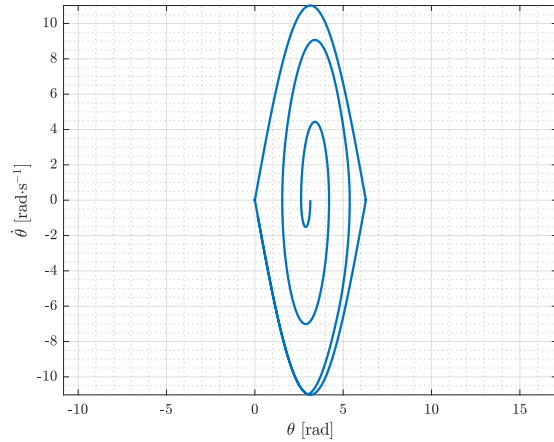
For these graphs  $k = 1.3$  to keep the motor current at acceptable levels. The motor current is shown in Figure 3.5 where the rolling RMS of  $i_a$  is used to approximate the continuous current load on the motor.

## Sign-Based Energy Control

There are other ways to satisfy Equation 3.17 than the control law suggested in Equation 3.18. To achieve maximal actuation a sign-function can be used to determine the direction of actuation along with a gain  $k$  to adjust for the limits of the actuator,

$$(3.22) \quad \ddot{x}_c = k \operatorname{sgn}(-E_\Delta \cos \theta \dot{\theta}) \quad ,$$

where  $\operatorname{sgn}$  is redefined to be one if it outputs zero, to avoid no actuation when starting at stable equilibrium. The gain is tuned to  $k = 2.7$  in the following simulation. Looking at the energy in Figure 3.6 this strategy seems to work really well. From the phase plot in Figure 3.7 it is evident that a near perfect heteroclinic orbit is reached.

**Figure 3.6:** Edelta2noConX**Figure 3.7:** phase2noConX

### Chapter 3. Swing-Up Design

In Figure 3.8 however, while the angle reaches the equilibrium as closely as possible without overshooting, this control law, as with the previous, does not account for position of the cart.

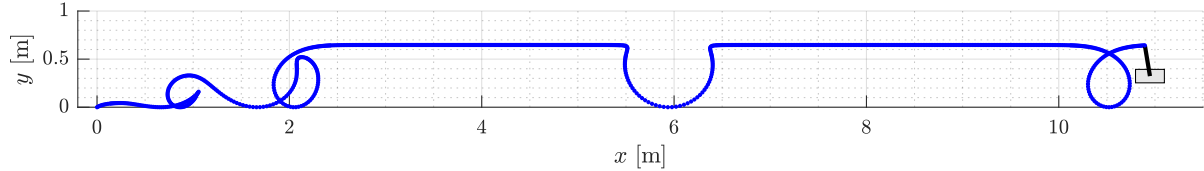


**Figure 3.8:** ani2noConX

However, the bigger problem with this control law is obvious from Figure 3.9, where excessive switching shows on the control output. This actuation behavior is not feasible in a real system and attempted implementation will cause chattering resulting in unwanted behavior and wear of the motor.

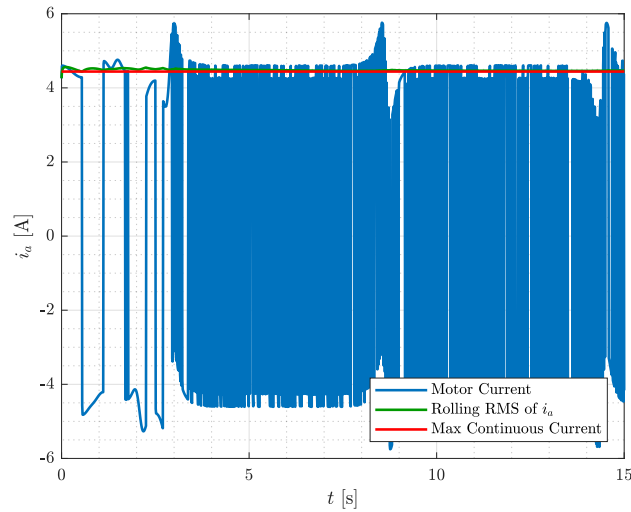


**Figure 3.9:** ia2noConX

It is possible to implement a less aggressive version of this idea by using a saturation function to approximate the sign function around zero,

$$(3.23) \quad \ddot{x}_c = k \operatorname{sat}\left(-\frac{1}{\varepsilon} E_\Delta \cos \theta \dot{\theta}\right) ,$$

where  $\varepsilon$  decides the slope of the saturation function around zero,

$$(3.24) \quad \operatorname{sat}\left(\frac{c}{\varepsilon}\right) = \begin{cases} \frac{c}{\varepsilon} & , \text{ if } \left|\frac{c}{\varepsilon}\right| \leq 1 \\ \operatorname{sgn}\left(\frac{c}{\varepsilon}\right) & , \text{ if } \left|\frac{c}{\varepsilon}\right| > 1 \end{cases} ,$$

where  $c$  is an input to the sat-function. In the simulation  $k = 2.7$  as before and  $\varepsilon = 0.01$  to avoid excessive switching while maintaining a relatively close approximation of the sign-function. This control strategy achieves the energy reference in about three seconds,

Figure 3.10, as is the case of the sign strategy, Figure 3.6. Further, from Figure 3.11, the system still reaches a near perfect heteroclinic orbit.

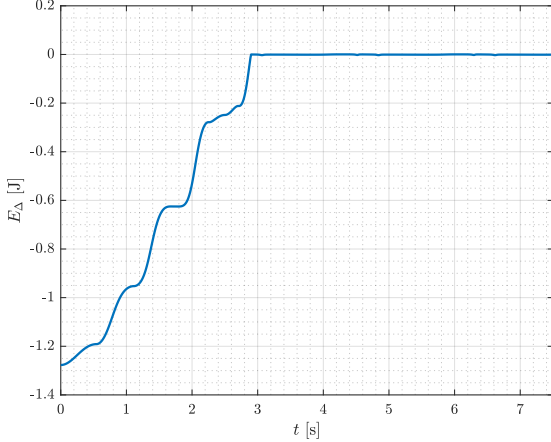


**Figure 3.10:** Edelta3noConX

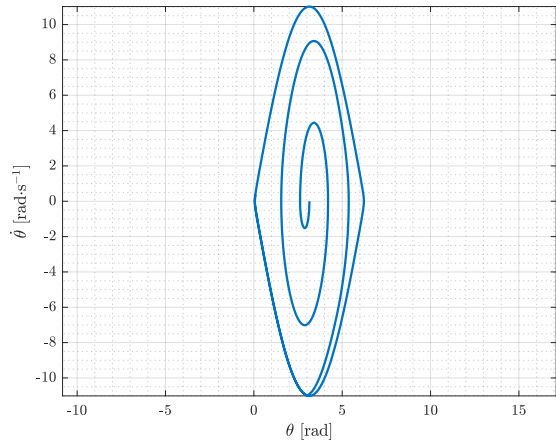


**Figure 3.11:** phase3noConX

The cart still drifts as expected, see Figure 3.12.

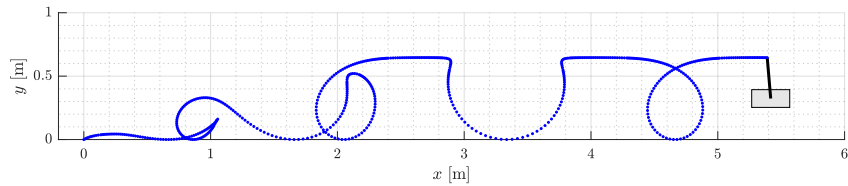


**Figure 3.12:** ani3noConX

The excessive switching on the control output is successfully avoided, see Figure 3.13, resulting in a much more realistic control signal compared to that in Figure 3.9.

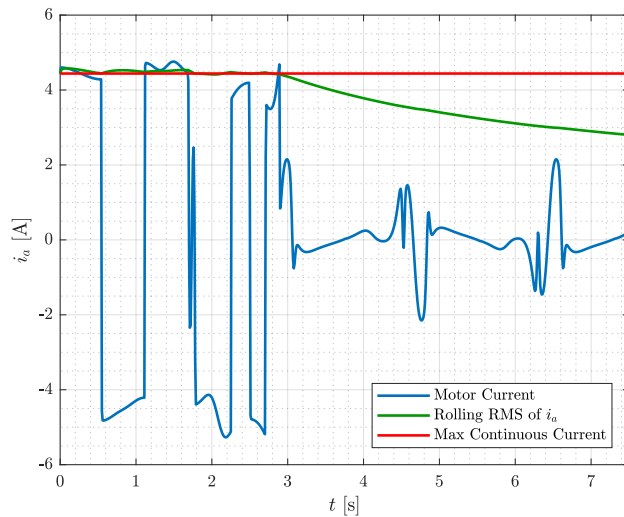


**Figure 3.13:** ia3noConX

## Sat-Based Energy Control

An other strategy to avoid the excessive switching of the sign-controller is presented here,

$$(3.25) \quad \ddot{x}_c = \text{sat}(-kE_{\Delta}\text{sgn}(\cos\theta\dot{\theta})) \quad ,$$

where the saturation function is saturates at the maximum/minimum allowed acceleration. The known limitation is  $i_{max} = 4.58$  as stated in Table 2.1, from which the maximum control,  $u$ , can be calculated,

$$(3.26) \quad u_{max} = \frac{k_{\tau}}{r} \quad ,$$

and finally by disregarding the pendulum behavior and cart friction from the dynamics in Equation 2.12,

$$(3.27) \quad a_{max} = \frac{u_{max}}{M+m} \quad .$$

As this is a crude estimation 0.2 is subtracted from the estimated  $a_{max}$  in following simulations to stay within the actuation limits. The saturation function is then,

$$(3.28) \quad \text{sat}(c) = \begin{cases} c & , \quad \text{if } |c| \leq a_{max} \\ \text{sgn}(c) a_{max} & , \quad \text{if } |c| > a_{max} \end{cases} ,$$

where  $c$  is the input to the sat-function. Again, the sign function is redefined to one in cases where it obtains a zero value. Choice of  $k$  in Equation 3.25 decides how aggressive the controller should be. Larger values of  $k$  drives the control into saturation faster thus actuating more like the sign-based controller in Equation 3.22. At lower values of  $k$  the operation will not reach saturation as fast thus behaving more like the first energy based controller in Equation 3.18. For an effective swing up behavior  $k = 200$  is used putting the control closer to that of the sign-based controller, which makes sense as this was the theoretically ideal option.

The performance in Figure 3.14 is similar to that in Figure 3.10 and again the system reaches a near perfect heteroclinic orbit in Figure 3.15.

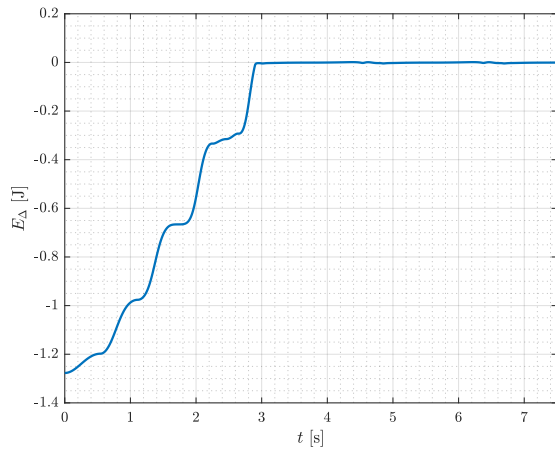


**Figure 3.14:** Edelta4noConX

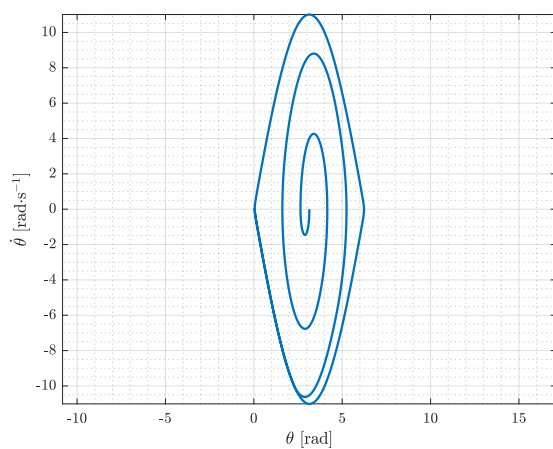


**Figure 3.15:** phase4noConX

The overall behavior also closely mimics that of Figure 3.12 as seen in Figure 3.16.

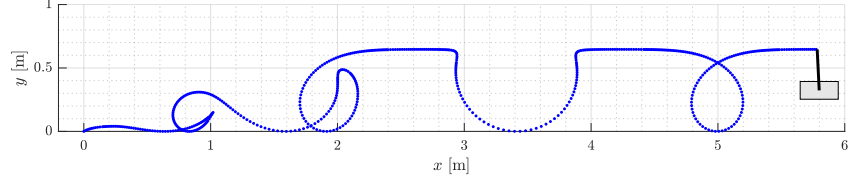


**Figure 3.16:** ani4noConX

There is however a slight difference in the control signal. In Figure 3.17 less switching occurs compared to Figure 3.13.

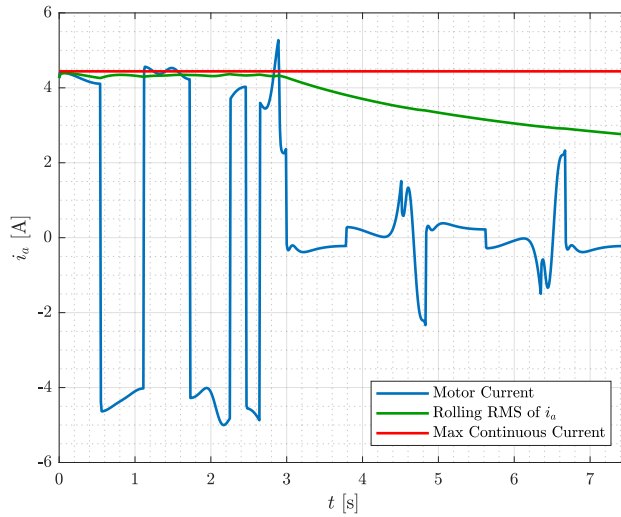


**Figure 3.17:** ia4noConX

Two of the four investigated controller designs are deemed good candidates, namely Equation 3.23 and page 15. The problem of controlling the cart position still remains. The performances of the two control law candidates are compared as they are subjected to the disturbance caused by added control on the cart position and velocity.

## Cart Position and Velocity Control

To solve the cart drifting problem along  $x$  a linear controller is designed and added to the control law,

$$(3.29) \quad \ddot{x}_c = \psi(x_1, x_3) + v(x_2, x_4) ,$$

where  $\psi(x_1, x_3)$  is the energy controller and  $v(x_2, x_4)$  is the linear controller. While these two controllers depend on different states, they still influence and act as unmodeled disturbances to each other. The position and velocity control,  $v(x_2, x_4)$ , adds and subtracts energy and therefore could cause the energy controller,  $\psi(x_1, x_3)$ , to overshoot. One solution to this potential problem could be to slightly lower the energy reference. However,

### Chapter 3. Swing-Up Design

swing-up is often designed with a slightly higher energy reference such that the catch controller has some entry velocity at the unstable equilibrium.

With these considerations in mind, the design of  $v(x_2, x_4)$  is proceeded. Considering the cart without friction and assuming that any influence of the pendulum and the energy control to be unmodeled disturbances of the system. This reduces the system to the mechanical drawing seen in Figure 3.18.

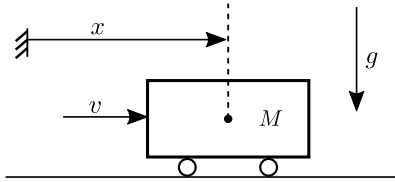


**Figure 3.18:** mechanicalDrawingSimple

The dynamics are then,

$$(3.30) \quad M\ddot{x} = v \quad ,$$

and selecting new states  $[x_1 \ x_2]^T = [x \ \dot{x}]^T$ , the linear state space is,

$$(3.31) \quad \begin{bmatrix} \dot{x}_1 \\ \dot{x}_2 \end{bmatrix} = \underbrace{\begin{bmatrix} 0 & 1 \\ 0 & 0 \end{bmatrix}}_A \begin{bmatrix} x_1 \\ x_2 \end{bmatrix} + \underbrace{\begin{bmatrix} 0 \\ \frac{1}{M} \end{bmatrix}}_B v \quad .$$

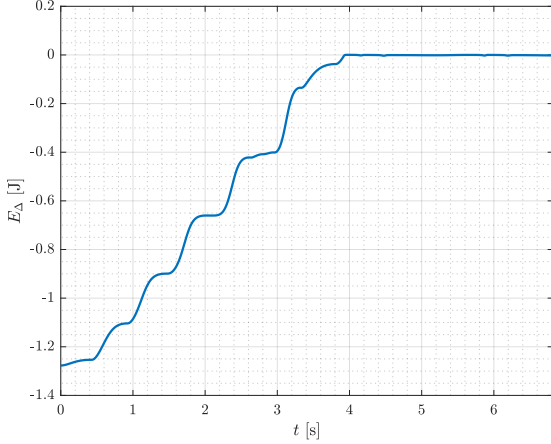
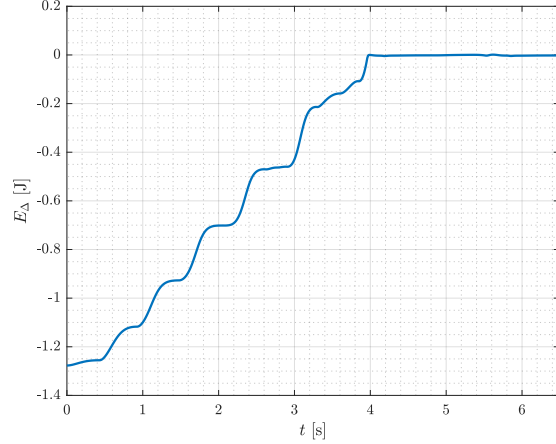
The closed loop poles are placed in  $p = [-1 \ -2]$  using matlab `place()`-command to obtain linear feedback gains,  $\mathbf{k}_1 = [10.5460 \ 15.8190]$ , resulting in the controller,

$$(3.32) \quad v = -\mathbf{k}_1 \mathbf{x} \quad ,$$

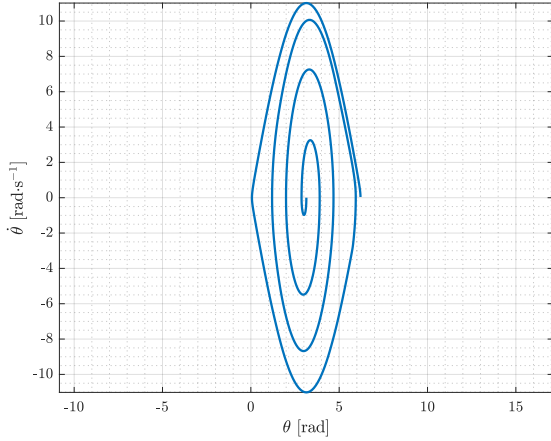
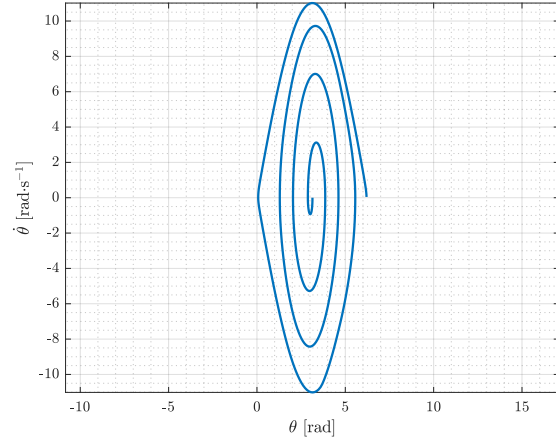
where  $\mathbf{x} = [x \ \dot{x}]^T$ , such that,

$$(3.33) \quad v(x_2, x_4) = -\mathbf{k}_1 [x_2 \ x_4]^T \quad ,$$

in terms of the full system. This control is added to both of the considered energy control approaches and simulations are run without changing any previously designed gains. Figure 3.19 shows the energy difference in the approximated sign approach while Figure 3.20 shows the sat-based approach. The approximated sign control approaches the reference slightly faster, however both reaches the reference at the same time.

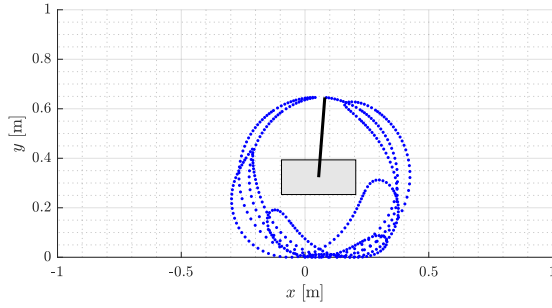

**Figure 3.19:** Edelta3ConX

**Figure 3.20:** Edelta4ConX

In the phase portraits, see Figure 3.21 and 3.22, both control strategies reaches the heteroclinic orbit. However the approximated sign approach comes slightly closer in the swing preceding the orbit. If it is close enough that a catch controller could catch it, one swing could be saved.

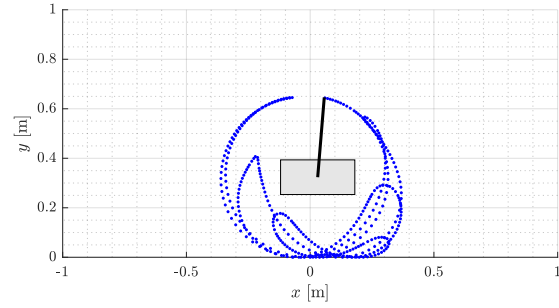

**Figure 3.21:** phase3ConX

**Figure 3.22:** phase4ConX

This fact is also seen in Figure 3.23 where the trace of the swing preceding the heteroclinic orbit reaches higher than in Figure 3.24. These figures also show that the linear control of the cart position and velocity successfully keeps the system within the accessible operating region of the real system.

### Chapter 3. Swing-Up Design



**Figure 3.23:** ani3ConX



**Figure 3.24:** ani4ConX

Figure 3.25 shows the actuation of the approximated sign approach, where the added linear control has caused less switching compared to Figure 3.13. In fact, both control strategies show very similar output when comparing to Figure 3.26. In both cases the RMS is lower than before the added linear controller. This could be tuned more tightly, but is left as a margin for now, with the possibility of further tuning during implementation.

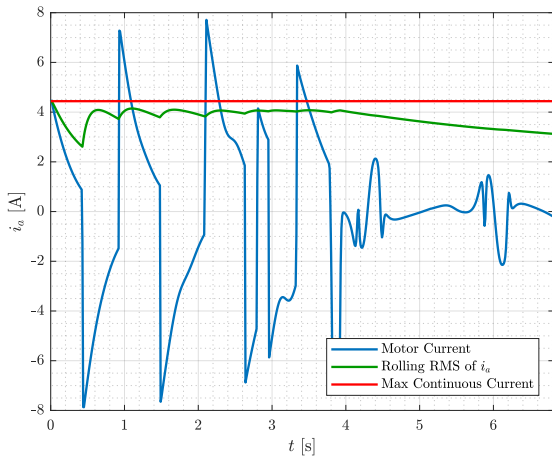


**Figure 3.25:** ia3ConX

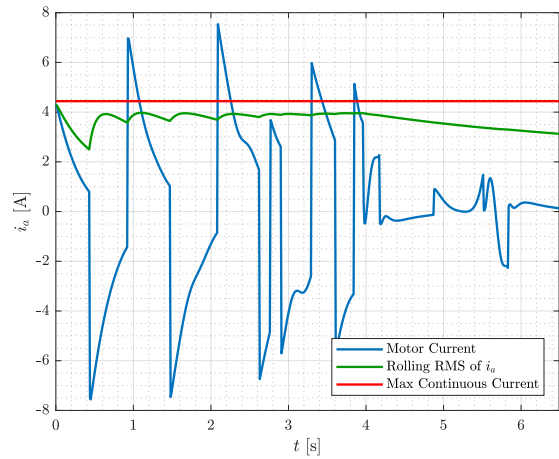


**Figure 3.26:** ia4ConX

Figure 3.27 and 3.28 show the position approaching zero as the energy control settles, which is ideal, as it means the energy controllers still have room to operate without fighting the linear feedback controller too much. Similarly, the oscillations around zero are necessary for the energy controller to keep its reference.

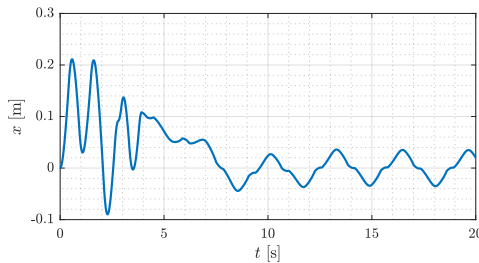


**Figure 3.27:** x3ConX

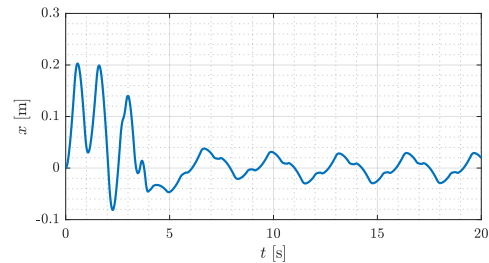


**Figure 3.28:** x4ConX

The same is seen for the velocity in Figure 3.29 and 3.30. These four graphs are simulated over longer time to show that the linear controller reaches its reference.

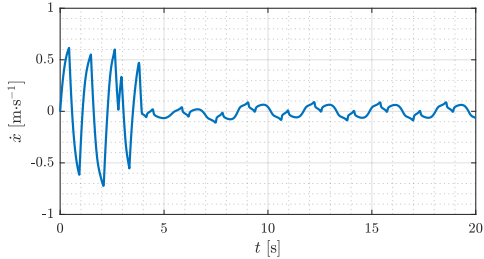


**Figure 3.29:** xDot3ConX

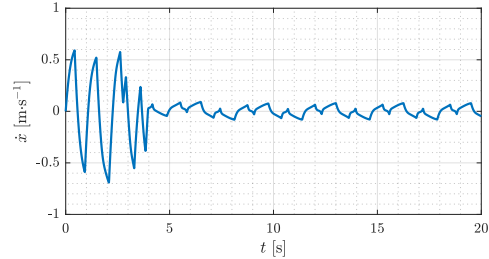


**Figure 3.30:** xDot4ConX

# **Part II**

## **Twin Pendulum**

# Bibliography

- [1] *Maxon RE Motor*. Oct. 8, 2018. URL: [https://www.maxonmotor.com/medias/sys\\_master/root/8825409470494/17-EN-133.pdf](https://www.maxonmotor.com/medias/sys_master/root/8825409470494/17-EN-133.pdf).
- [2] Avago Technologies. *HEDM-55xx/560x & HEDS-55xx/56xx*. Aug. 15, 2018. URL: [https://www.infineon.com/dgdl/Infineon-Encoder\\_HEDS-5540-A14-AP-v01\\_00-EN.pdf?fileId=5546d46147a9c2e40147d3d593970357](https://www.infineon.com/dgdl/Infineon-Encoder_HEDS-5540-A14-AP-v01_00-EN.pdf?fileId=5546d46147a9c2e40147d3d593970357).
- [3] *Maxon Controller*. Aug. 15, 2018. URL: <https://www.maxonmotor.com/maxon/view/product/control/Servoerstaerker-4-Q-DC/201583>.
- [4] *sparkfun Teensy 3.6*. Aug. 15, 2018. URL: <https://www.sparkfun.com/products/14057>.
- [5] *HCTL-2021 PLC Avago Datasheet*. Aug. 15, 2018. URL: <https://datasheet.octopart.com/HCTL-2021-PLC-Avago-datasheet-7580518.pdf>.
- [6] *K66 Sub-Family Reference Manual*. Aug. 15, 2018. URL: <https://cdn.sparkfun.com/datasheets/Dev/Arduino/Boards/K66P144M180SF5RMV2.pdf>.
- [7] Jonas Ørndrup Jesper H. Hørgensen. *Non-linear Control and Machine Learning on an Inverted Pendulum on a Cart*. Master Thesis. 2018.
- [8] Niels Skov Vestergaard. *Sliding Mode Stabilization and Phase Plane Trajectory Planning for a Cart Pendulum System*. 9<sup>th</sup> Semester Project. 2018.
- [9] Rafael Wisniewski. *Mechanical Systems II. Lagrange Mechanics*. Aalborg University, 2013.
- [10] Charles M. Close, Dean K. Frederick, and Jonathan C. Newell. *Modeling and Analysis of Dynamic Systems*. Wiley, 2001.
- [11] H. Olsson et al. *Friction Models and Friction Compensation*. Nov. 28, 1997.
- [12] Mark W. Spong, Seth Hutchinson, and M. Vidyasagar. *Robot Dynamics and Control*. 2nd ed. Wiley, 2005.
- [13] Lorenzo Sciavicco and Bruno Siciliano. *Modelling and Control of Robot Manipulators*. 2nd ed. Lorenzo Sciavicco and Bruno Siciliano. London: Springer, 2012.
- [14] Karl Johan Åström and Katsuhisa Furuta. “Swinging up a pendulum by energy control”. In: *Automatica* 36.2 (2000), pp. 287–295.

# List of Corrections

Note: brush up on stability criteries . . . . .	9
Note: include small section on heteroclinic orbit . . . . .	11
Note: remember a section on friction compensation . . . . .	11